Available online at www.sciencedirect.com

ScienceDirect

Ceramics International 39 (2013) 9385–9390

CERAMICS INTERNATIONAL

www.elsevier.com/locate/ceramint

Microstructure, temperature stability and electrical properties of ZnO-modified $Pb(Ni_{1/3}Nb_{2/3})O_3$–$Pb(Fe_{1/2}Nb_{1/2})O_3$–$Pb(Zr_{0.3}Ti_{0.7})O_3$ piezoelectric ceramics

Jianzhou Du, Jinhao Qiu*, Kongjun Zhu*, Hongli Ji

State Key Laboratory of Mechanics and Control of Mechanical Structures, Nanjing University of Aeronautics and Astronautics, Nanjing 210016, PR China

Received 2 March 2013; received in revised form 1 May 2013; accepted 1 May 2013
Available online 23 May 2013

Abstract

Quaternary piezoelectric ceramics $Pb(Ni_{1/3}Nb_{2/3})O_3$–$Pb(Fe_{1/2}Nb_{1/2})O_3$–$Pb(Zr_{0.3}Ti_{0.7})O_3$–xZnO (PNN–PFN–PZT–xZ, $x=0.0$–0.08 in molar ratio) were prepared by the conventional mixed-oxide method. The effects of ZnO content on the microstructure and piezoelectric properties were systematically investigated. Increasing ZnO additive promotes the phase structure transformation from rhombohedral to tetragonal, indicating the presence of the morphotropic phase boundary in the ZnO-modified PNN–PFN–PZT system. The results show that ZnO doping significantly improves the coercive field (E_c), Curie temperature (T_c), and temperature stability ($\Delta f_r/f_{r\ 30\ ^\circ C}$, $\Delta d_{31}/d_{31\ 30\ ^\circ C}$) of the PNN–PFN–PZT–$x$Z ceramics, although the piezoelectric constant (d_{33}, d_{31}) decreases slightly with increasing ZnO content. Taking into consideration the piezoelectric property and temperature stability, the obtained ceramic sample with $x=0.04$ exhibited favorable properties, which are listed as follows: $d_{33}=810$ pC/N, $k_p=0.647$, $\varepsilon_r=6243$, $\tan\delta=2.74\%$, $E_c=4.7$ kV/cm, and $T_c=136$ °C.

Keywords: A. Sintering; C. Dielectric properties; C. Piezoelectric ceramics; D. ZnO

1. Introduction

Lead zirconate titanate (PZT) ceramics have attracted tremendous attention since the 1970s due to their excellent piezoelectric and electromechanical properties near the morphotropic phase boundary (MPB) [1–4]. Besides, the PZT-based ceramics are widely employed in many applications, ranging from electrostrictive actuators and transducers, to sensors and ultrasonic devices [5–9]. Typically, the PZT-based relaxor ferroelectrics have a general formula of $Pb(B_1B_2)O_3$ (where B_1 stands for Mg^{2+}, Ni^{2+}, Zn^{2+}, Fe^{3+}, Mn^{4+}, or Sn^{4+}; and B_2 stands for Nb^{5+}, Sb^{5+}, or W^{6+}). In an effort to enhance piezoelectric activities and stabilize the perovskite structure, a relaxor type $Pb(B_1B_2)O_3$-PZT ceramic was developed. Up to now, numerous solid solution systems comprising normal and relaxor ferroelectrics with outstanding piezoelectric and dielectric properties have been developed, such as $0.5Pb(Zn_{1/3}Nb_{2/3})O_3$–$0.5Pb(Zr_{0.47}Ti_{0.53})O_3$ [10], $0.3Pb(Ni_{1/3}Nb_{2/3})O_3$–$x$PbTiO$_3$–$(0.7-x)$PbZrO$_3$ ($x=0.33$–0.43) [11], $Pb(Mn_{1/3}Sb_{2/3})O_3$–$Pb(Zn_{1/3}Nb_{2/3})O_3$–$Pb(Zr_{0.52}Ti_{0.48})O_3$ [12], $Pb(Sn_{1/3}Sb_{2/3})O_3$–$Pb(Zn_{1/3}Nb_{2/3})O_3$–PbZrO$_3$–PbTiO$_3$ [13], and so on.

Relaxor-type PZT-based ceramics doped with numerous oxides (ZnO, CuO, La_2O_3, Fe_2O_3, CeO_2, MnO_2, etc.) have been intensively investigated to further improve the physical and electrical properties for actual industrial applications. For example, Zhang et al. [14] found that Ce-doped PNW–PMN–PZT ceramics with good temperature stability achieve favorable piezoelectric and dielectric properties ($d_{33}=388$ pC/N, $k_p=0.6$). Kang et al. [15] investigated the effect of Y_2O_3 additives on the electrical properties of PNN–PZT ceramics, and both good ferroelectric and pyroelectric properties ($2P_r=21$ μC/cm^2, $2E_c=7.7$ kV/cm, $F_D=452$ μC/cm^2 K) were obtained for the 1.0 mol% Y^{3+} doped sample. Gao et al. [16] found that the PMN–PNN–PZT ceramics modified with Zn^{2+} and Li^+ ions exhibited excellent electrical properties ($d_{33}=397$

*Corresponding authors. Tel./fax: +86 25 84891123.
E-mail addresses: qiu@nuaa.edu.cn (J. Qiu), kjzh@nuaa.edu.cn (K. Zhu).

0272-8842/$ - see front matter © 2013 Elsevier Ltd and Techna Group S.r.l. All rights reserved.
http://dx.doi.org/10.1016/j.ceramint.2013.05.055

pC/N, ε_r=2628) and high Curie temperature (T_c=251 °C) at a low sintering temperature of 960 °C. Yan et al. [17] studied the effect of MnO_2 on the phase structure and ferroelectric behavior of PMN–PZT ceramics and found that the Mn ion substitution on Zr and Ti sites induced a hardening effect.

In our previous report [18], PNN–PZT ternary ceramics doped with appropriate amount of Fe_2O_3 exhibited high piezoelectric constant (d_{33} > 870 pC/N), large planar electromechanical coupling factor (k_p > 0.7), high dielectric constant (ε_r > 5690), and low dielectric loss (tan δ < 3%), yet T_c is only 120 °C near the MPB area, seriously restricting its potential application at high temperature. Hence, the temperature stabilities of PZT-based piezoelectric properties have also been studied [19,20]. It was reported that ZnO doping can effectively improve thermal stability of PZT–PMnN [21,22], Mn^{4+}/Nb^{5+}-modified PZT [23], PZT–PMnS [24], and PMW–PNN–PZT [25] ceramics with good piezoelectric and dielectric properties. Similar results have also been found in the ZnO-doped lead-free KNN-based ceramics [26–28].

In this work, ZnO was used as an additive in PNN–PFN–PZT multicomponent system to improve the dielectric properties and Curie temperature. Herein, an effort has been made to provide feasible candidates with both excellent piezoelectric and temperature stabilities for practical applications. The effects of ZnO content on the microstructure, electrical properties, and temperature stabilities of the ceramics were studied.

2. Experimental procedure

The ceramics with compositions of $0.5Pb(Ni_{1/3}Nb_{2/3})O_3$–$0.05Pb(Fe_{1/2}Nb_{1/2})O_3$–$0.45Pb(Zr_{0.3}Ti_{0.7})O_3$+$x$ZnO (abbreviated as PNN–PFN–PZT+xZ, where x=0.0, 0.02, 0.04, 0.06, and 0.08) were prepared by a conventional mixed-oxide method. Reagent-grade PbO, NiO, Nb_2O_5, ZrO_2, TiO_2, Fe_2O_3, and ZnO oxide powders were used as the starting materials. Excess 1 wt % PbO was added mainly to compensate for the lead loss at a high temperature and suppress the pyrochlore phase during the sintering process. The mixed powders were ball milled in alcohol for 12 h with agate balls and jar. The slurry was dried, calcined in an alumina crucible at 1050 °C for 4 h, and re-milled for 10 h. The powders were dried and uniaxially pressed into disks at 200 MPa using polyvinyl alcohol (PVA) as a binder. All samples were sintered at 800 °C for 5 h to burn off the PVA, and then sintered at 1200 °C for 2 h in a sealed aluminum crucible.

The bulk densities (ρ) of the sintered samples were measured through the Archimedes method. The crystal structures of the samples were determined at room temperature by X-ray diffraction (XRD, D/Max-2500, Rigaku, Japan). The surface morphologies were observed by a scanning electron microscope (SEM, JMS-5610LV, Tokyo, Japan). Silver electrodes were coated on both sides of polished ceramic disks, which were then fired at 550 °C for 10 min. The samples were poled in silicone oil at 60 °C by applying a DC electric field of 2 kV/mm for 20 min.

The piezoelectric constant (d_{33}) was measured through a quasistatic piezoelectric d_{33} meter (ZJ-3A, Institute of Acoustics, Chinese Academy of Sciences, China). The electromechanical coupling factor (k_p, k_{31}), piezoelectric constant (d_{31}), and mechanical quality factor (Q_m) were determined through the resonance and anti-resonance method with an LCR analyzer (HP4294A, Agilent, America) based on IEEE standards. The Curie temperature (T_c) and temperature stability of the ceramic samples were analyzed using an HP4294A precision impedance analyzer in a controlled furnace at a heating rate from room temperature to 300 °C. The polarization hysteresis loops (P–E) were measured using a ferroelectric analyzer system (TF2000, aixACCT Systems GmbH, Germany) at 5 Hz based on a modified Sawyer-Tower circuit.

3. Results and discussion

3.1. Microstructure analysis

Fig. 1 shows the XRD patterns of the PNN–PFN–PZT+xZ ceramics with different ZnO contents sintered at 1200 °C. All samples exhibit a pure ABO_3 perovskite structure without obvious pyrochlore or secondary phase (e.g., $Pb_2Nb_2O_7$, $Pb_3Nb_4O_{13}$, and $Pb_5Nb_4O_{15}$). It is indicated that ZnO can diffuse into the PNN–PFN–PZT lattice and form a new solid solution. The previous studies [13,29–31] have demonstrated that the lower symmetrical crystal structures can be indexed by splitting the diffraction peaks (hkl), such as a single (200) peak indexed as rhombohedral symmetry, or (110) and (200) peaks splitting indexed as a tetragonal symmetry. For further analysis of the effect ZnO doping on the phase structure of the PNN–PFN–PZT +xZ ceramics, (002) and (200) peaks were zoomed in the 2θ range of 44–46° as shown in Fig. 1(b). The pure PNN–PFN–PZT ceramics, presenting the single peak of $(200)_R$, are primarily indexed as the rhombohedral phase. It can be observed that the $(200)_R$ peak gradually splits into $(002)_T$ and $(200)_T$ peaks with the increasing of ZnO content, indicating a phase shift from rhombohedral to tetragonal near the MPB. The rhombohedral and tetragonal phases coexist as x increases from 0.04 to 0.06,

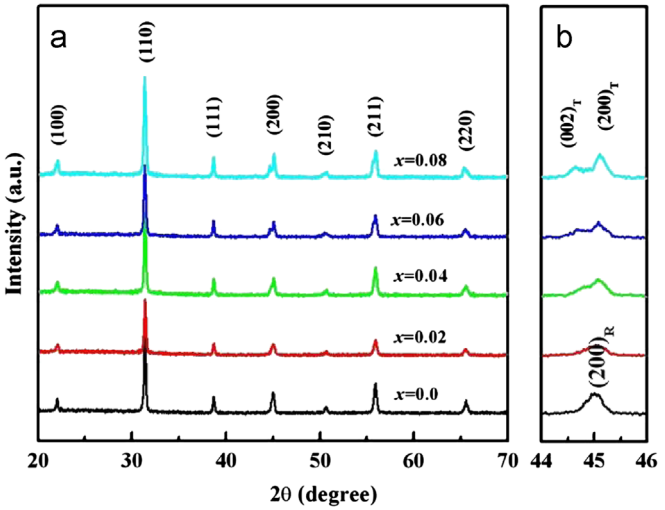

Fig. 1. XRD patterns of PNN–PFN–PZT+xZ (x=0.0–0.08) ceramics with different ZnO contents in the 2θ range of 20–70° (a) and (b) enlarged (002) and (200) peaks within 44–46° sintered at 1200 °C.

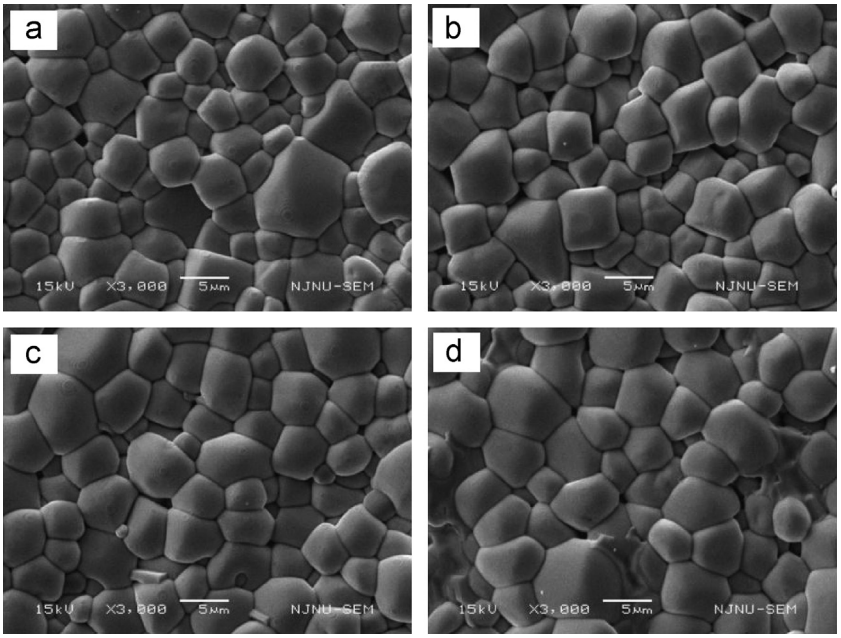

Fig. 2. SEM micrographs of PNN–PFN–PZT+xZ ceramics with different ZnO contents sintered at 1200 °C for 2 h: (a) $x=0.0$, (b) $x=0.02$, (c) $x=0.04$ and (d) $x=0.08$.

Table 1
The physical properties of PNN–PFN–PZT–xZ ceramics sintered at 1200 °C for 2 h.

Sample	ρ (kg/m^3)	ε_r	tan δ (%)	d_{33} (pC/N)	k_p	d_{31} (pC/N)	k_{31}	Q_m	T_c (°C)
$x=0.0$	7965	5697	2.82	885	0.707	−367	0.422	44.6	107
$x=0.02$	7908	6101	2.88	831	0.646	−341	0.365	46.1	122
$x=0.04$	7881	6243	2.74	810	0.647	−342	0.357	46.7	136
$x=0.06$	7831	5670	2.49	750	0.635	−320	0.352	56.8	143
$x=0.08$	7814	5159	2.25	657	0.608	−289	0.336	62.7	154

which is similar to MPB behavior concerning the PZT–PMS–PZN, PSN–PZN–PZT, and PZT–PZN–PNN ceramics [12,13,19]. This phase transition can be ascribed to the Zn^{2+} ions diffusion into the B-site ions of the BO_6 octahedron.

Fig. 2 shows the SEM micrographs of the PNN–PFN–PZT +xZ ceramics with different ZnO contents sintered at 1200 °C for 2 h. The PNN–PFN–PZT ceramic without ZnO doping shows clear grain boundary and dense microstructure with a reduced amount of porosity (Fig. 2(a)). The bulk density decreases slightly with the increasing ZnO content, while the grain size remains almost unchanged. The density in the range of 94–96% of the theoretical value can also be achieved in all samples (Table 1). However, with further increase of x to 0.08, the excessive ZnO segregates at the grain boundary and forms a liquid phase with the lower melting oxides such as PbO, NiO, and Nb_2O_5. This result corresponds well with the SEM photographs shown in Fig. 2(c, d). This phenomenon is also consistent with those in widely reported ZnO-doped PZT–PMnN [22], PMS–PZT [24], and PMW–PNN–PZT [25] ceramic systems.

3.2. Piezoelectric, dielectric, and ferroelectric properties

Fig. 3 shows the piezoelectric and dielectric properties of the PNN–PFN–PZT+xZ ceramics sintered at 1200 °C as a function of ZnO content x. With the ZnO content x increasing from 0.0 to 0.08, both d_{33} and k_p decrease gradually from 885 pC/N and 0.707 to 657 pC/N and 0.608, respectively, as shown in Fig. 3(a). The relative dielectric constant ε_r reached a maximum value of 6243 at $x=0.04$, and then decreases with the increasing ZnO content. The varying trend of the tan δ versus x is similar to that of the ε_r, and the peak value of tan δ is 2.88% at $x=0.02$. The enhancement of the dielectric property is caused mainly by the phase transition behavior near the MPB. The variations of densities, piezoelectric constants, and dielectric constants are listed in Table 1 to comprehensively evaluate the performance of the obtained ceramics. It is shown that the PNN–PFN–PZT+xZ ceramics with $x=0.04$ exhibit excellent dielectric and piezoelectric properties ($\varepsilon_r=6243$, tan $\delta=2.74\%$, $d_{33}=810$ pC/N, $d_{31}=-342$ pC/N, $k_p=0.647$, $k_{31}=0.357$, and $Q_m=46.7$) at room temperature.

Fig. 4 shows the P–E hysteresis loops of the PNN–PFN–PZT+xZ ceramics measured at room temperature. It is shown that both pure and Zn-doped ceramic samples exhibit square-like well-saturated hysteresis loops. The remnant polarization (P_r) and saturation polarization (P_s) of pure ceramics are 22.4 and 28.3 μC/cm^2, respectively, and its coercive field (E_c) is 3.8 kV/cm. With the increase of ZnO content, the values of both P_r and P_s gradually decrease from 21.7 and 27.5 μC/cm^2 at $x=0.02$ to 20.5 and 26.3 μC/cm^2 at $x=0.08$, respectively,

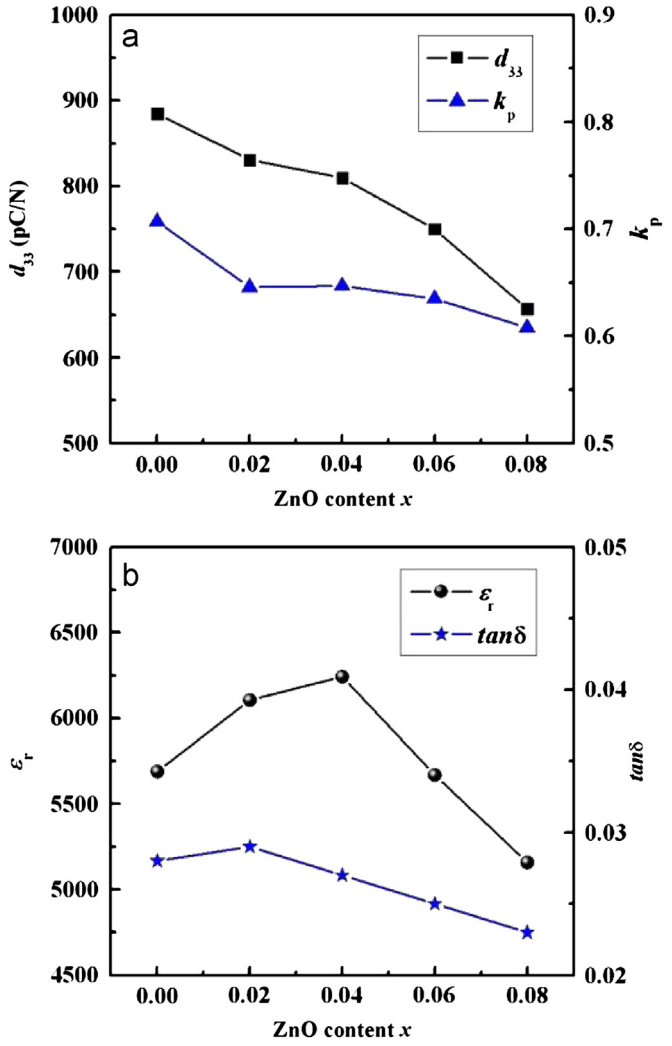

Fig. 3. The d_{33}, k_p, ε_r and tan δ of PNN–PFN–PZT+xZ ceramics sintered at 1200 °C as a function of ZnO content.

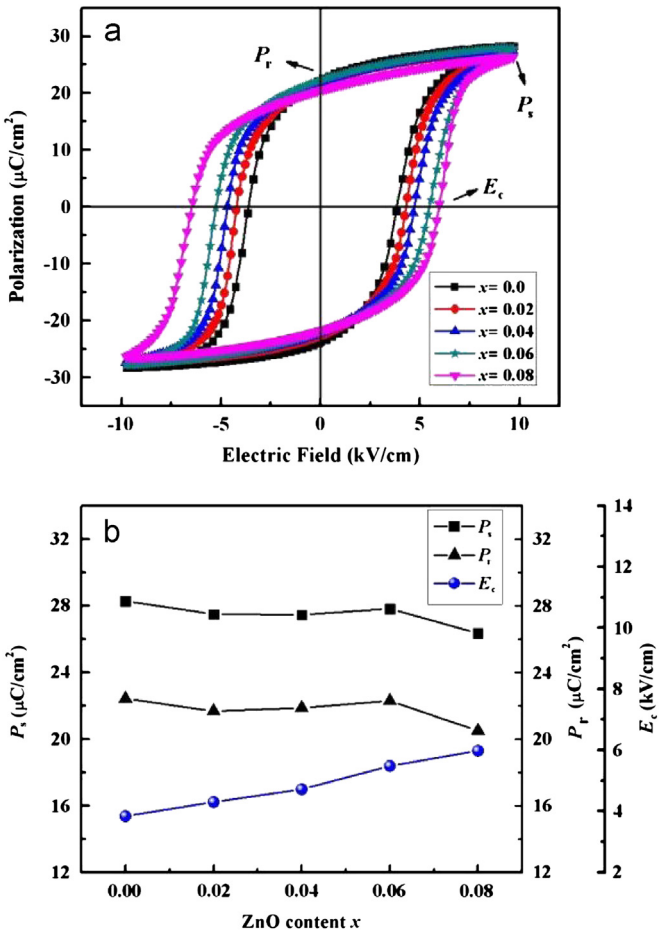

Fig. 4. (a) Polarization–electric field (P–E) hysteresis loops and (b) the values of P_s, P_r, and E_c of PNN–PFN–PZT+xZ ceramics sintered at 1200 °C as a function of ZnO content.

as shown in Fig. 4(b). In addition, the E_c value shows an increasing trend with increase of ZnO content, and the corresponding values are 4.3, 4.7, 5.5, and 6.0 kV/cm for PNN–PFN–PZT+xZ with x=0.02, 0.04, 0.06 and 0.08, respectively. It is indicated that the domain switching becomes more difficult accompanied by a higher Zn^{2+} ion concentration, which may be attributed to the increased amount of the tetragonal phase and the existence of the liquid phase in the grain boundary.

3.3. Temperature stability

Fig. 5 shows the temperature dependence of ε_r and tan δ of the PNN–PFN–PZT+xZ ceramics measured at 1 kHz. As can be seen all samples exhibit relaxor dielectric behaviors as characterized by the diffused dielectric peaks, and ε_r and tan δ are strongly influenced by ZnO content. The Curie temperature (T_c) gradually increases from 107 °C to 136 °C and 154 °C as x increases from 0.0 to 0.04 and 0.08, respectively. Meanwhile, the corresponding maximum dielectric constants ε_{max} are 23,930, 223,817, and 27,470. The T_c shifting to a higher temperature with increasing ZnO content may be attributed to the fact that T_c of PZN (~140 °C) is higher than those of PNN (~−120 °C) and PFN (~110 °C). It should be noted that the maxima of tan δ for all PNN–PFN–PZT+xZ ceramics are lower than 7% near their Curie temperature.

In order to further demonstrate the effect of ZnO doping on the temperature stability of PNN–PFN–PZT ceramics, the temperature coefficients ($\Delta f_r/f_{r\ 30\ °C}$ and $\Delta d_{31}/d_{31\ 30\ °C}$) of the resonant frequency (f_r) and the piezoelectric constant (d_{31}) were measured in temperatures ranging from 30 °C to 140 °C; the equation is as follows:

$$\text{temperature coefficient } \frac{\Delta P}{P_1(T_1)} = \frac{P_2(T_2) - P_1(T_1)}{P_1(T_1)} \times 100\%,$$

where $P_2(T_2)$ and $P_1(T_1)$ are the measured electrical parameters at T_2 and T_1. Fig. 6 shows the temperature coefficients of f_r and d_{31} for the PNN–PFN–PZT+xZ ceramics as a function of temperature. The $\Delta f_r/f_{r\ 30\ °C}$ of pure PNN–PFN–PZT ceramics initially decreased slightly and then increased to 11.8% at 100 °C with the increase of the ambient temperature (T) as shown in Fig. 6(a). The $\Delta f_r/f_{r\ 30\ °C}$ of the ZnO-doped samples increased monotonically with increasing ambient temperature.

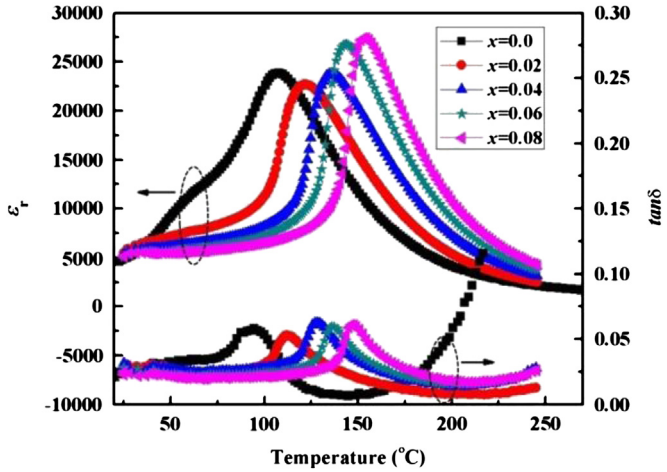

Fig. 5. Temperature dependence of ε_r and tan δ for PNN–PFN–PZT+xZ ceramics with different ZnO contents sintered at 1200 °C measured at 1 kHz.

Here, the slope of $\Delta f_r/f_{r\ 30\ °C}$ versus T decreases gradually with the increased ZnO content, indicating that the temperature stability of the resonant frequency can be improved through ZnO doping. Zhang et al. [32] insisted that the temperature stability is closely related to the performance of the PZT ceramics.

Fig. 6(b) shows the $\Delta d_{31}/d_{31\ 30\ °C}$ of the PNN–PFN–PZT+xZ ceramics as a function of temperature. The temperature coefficient $\Delta d_{31}/d_{31\ 30\ °C}$ exhibits an inverse tendency compared with the $\Delta f_r/f_{r\ 30\ °C}$ for all samples. The $\Delta d_{31}/d_{31\ 30\ °C}$ for the sample at $x=0.0$ initially slightly increases, and then decreases sharply by about −50% at T, ranging from 30 °C100 °C. d_{31} rapidly decreases, especially at around its Curie temperature ($T_c=107$ °C). The slopes of $\Delta d_{31}/d_{31\ 30\ °C}$ versus T decrease with the increase in content of ZnO, indicating the improvement of temperature stability with the increased ZnO content. The enhanced temperature stability can be related to the domain-wall activity and the domain structure [19,21,32]. Therefore, the ZnO-modified PNN–PFN–PZT ceramics possess high piezoelectric properties and good temperature stability.

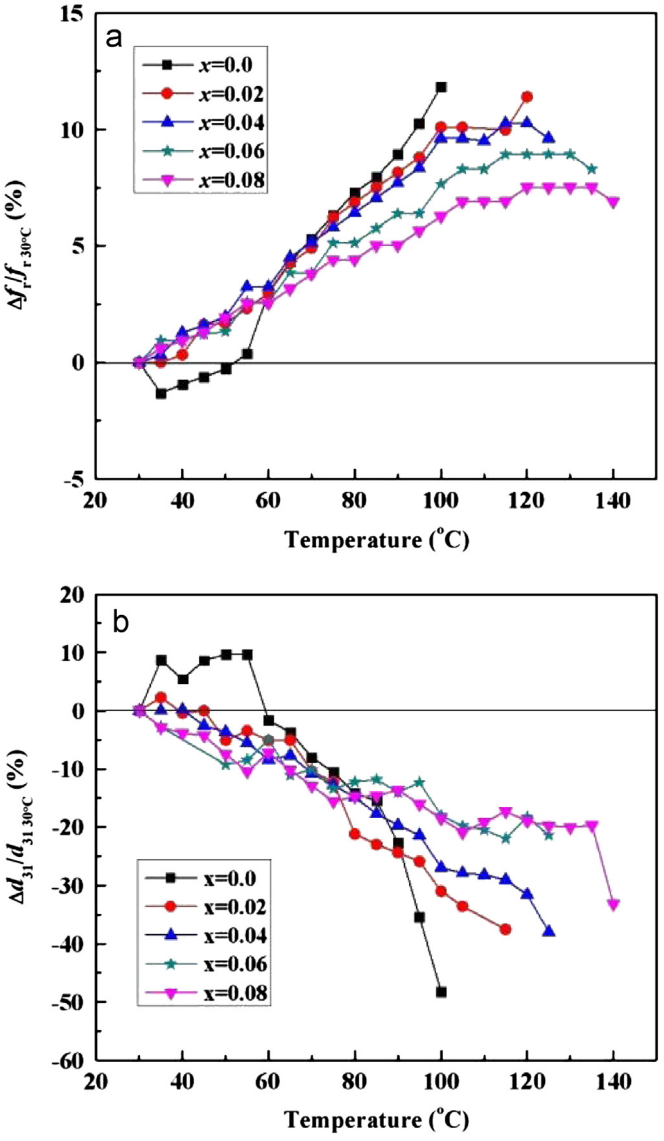

Fig. 6. Temperature dependence of (a) $\Delta f_r/f_{r\ 30\ °C}$ and (b) $\Delta d_{31}/d_{31\ 30\ °C}$ and $\Delta k_{31}/k_{31\ 30\ °C}$ for PNN–PFN–PZT+xZnO ceramics as a function of temperature.

4. Conclusions

PNN–PFN–PZT+xZnO ceramics with pure perovskite structure have been fabricated through the conventional ceramic sintering technique. All ceramics exhibit pure perovskite structure and the phase structure changes from rhombohedral to tetragonal on varying ZnO content. The relative dielectric constant ε_r achieves its maximum at $x=0.04$. The piezoelectric constant d_{33} and the planar electromechanical coupling factor k_p gradually decreased, while the mechanical quality factor Q_m and the coercive field E_c gradually increased with the increase of ZnO content, which should be attributed to the presence of the MPB and the hardening effect. The Curie temperature T_c exhibited an obvious increasing trend with the increased ZnO content. The temperature coefficients of $\Delta f_r/f_{r\ 30\ °C}$ and $\Delta d_{31}/d_{31\ 30\ °C}$ showed the inverse tendency and a flat temperature behavior for the ZnO-doped samples. The PNN–PFN–PZT +xZ ceramics with $x=0.04$ exhibited optimal properties: d_{33}, k_p, ε_r, tan δ, Q_m, E_c, and T_c are 810 pC/N, 0.647, 6243, 2.74%, 46.7, 4.7 kV/cm and 136 °C, respectively. Finally, the addition of ZnO significantly improved the temperature stability of the electrical properties for the PNN–PFN–PZT ceramics.

Acknowledgments

This work was supported by the National Natural Science Foundation of China (90923029, 51161120326), the Program for Changjiang Scholars and Innovative Research Team in University (IRT0968), the Funding for Outstanding Doctoral Dissertation in NUAA (BCXJ11-02), the Program for New Century Excellent Talents in University (NCET-10-0070), the Funding of Jiangsu Innovation Program for Graduate Education (CXZZ11-0194) and the PAPD of Jiangsu Higher Education Institutions.

References

[1] N. Vittayakorn, S. Uttiya, G. Rujijanagul, D.P. Cann, Dielectric and ferroelectric characteristics of 0.7PZT–0.3PZN ceramics substituted with Sr, Journal of Physics D: Applied Physics 38 (2005) 2942–2946.

[2] N. Vittayakorn, G. Rujijanagul, T. Tunkasiri, Perovskite phase formation and ferroelectric properties of the lead nickel niobate–lead zinc niobate–lead zirconate titanate ternary system, Journal of Materials Research 18 (2003) 2882–2889.

[3] B.K. Gan, K. Yao, Structure and enhanced properties of perovskite ferroelectric PNN–PZN–PMN–PZ–PT ceramics by Ni and Mg doping, Ceramics International 35 (2009) 2061–2067.

[4] B. Fang, Q. Du, D. Wu, L. Zhou, Y. Shan, K. Tezuka, H. Imoto, Structural and electrical properties of $0.56Pb(Ni_{1/3}Nb_{2/3})O_3$–$0.10Pb(Zn_{1/3}Nb_{2/3})O_3$–$0.34PbTiO_3$ ceramics prepared by different ceramic processings, Ceramics International 37 (2011) 707–713.

[5] R. Guo, L.E. Cross, S.E. Park, B. Noheda, D.E. Cox, G. Shirane, Origin of the high piezoelectric response in $PbZr_{1-x}Ti_xO_3$, Physical Review Letters 84 (2000) 5423–5426.

[6] B. Jaffe, R.S. Roth, S. Marzullo, Piezoelectric properties of lead zirconate–lead titanate solid–solution ceramics, Journal of Applied Physics 25 (1954) 809–810.

[7] F.P. Sun, Z. Chaudhry, C. Liang, C.A. Rogers, Truss structure integrity identification using PZT sensor–actuator, Journal of Intelligent Material Systems and Structures 6 (1995) 134–139.

[8] Y.B. Jeon, R. Sood, J.h. Jeong, S.G. Kim, MEMS power generator with transverse mode thin film PZT, Sensors and Actuators A 122 (2005) 16–22.

[9] T. Bove, W. Wolny, E. Ringgaard, A. Pedersen, New piezoceramic PZT–PNN material for medical diagnostics applications, Journal of the European Ceramic Society 21 (2001) 1467–1472.

[10] L.M. Chang, Y.D. Hou, M.K. Zhu, H. Yan, Effect of sintering temperature on the phase transition and dielectrical response in the relaxor-ferroelectric-system 0.5PZN–0.5PZT, Journal of Applied Physics 101 (2007) 034101.

[11] R. Cao, G. Li, J. Zeng, S. Zhao, L. Zheng, Q. Yin, The piezoelectric and dielectric properties of $0.3Pb(Ni_{1/3}Nb_{2/3})O_3$–$xPbTiO_3$–$(0.7-x)PbZrO_3$ ferroelectric ceramics near the morphotropic phase boundary, Journal of the American Ceramic Society 93 (2010) 737–741.

[12] Z. Yang, H. Li, X. Zong, Y. Chang, Structure and electrical properties of PZT–PMS–PZN piezoelectric ceramics, Journal of the European Ceramic Society 26 (2006) 3197–3202.

[13] S. Zhao, H. Wu, Q. Sun, Study on PSN–PZN–PZT quaternary piezoelectric ceramics near the morphotropic phase boundary, Materials Science and Engineering B 123 (2005) 203–210.

[14] R. Zhang, Z. Yang, X. Chao, C. Kang, Effects of CeO_2 addition on the piezoelectric properties of PNW–PMN–PZT ceramics, Ceramics International 35 (2009) 199–204.

[15] S.H. Kang, D.S. Lee, S.Y. Lee, I.W. Kim, J.S. Kim, E.C. Park, J.S. Lee, Pyroelectric and piezoelectric properties of yttrium-doped $0.15[Pb(Ni_{1/3}Nb_{2/3})O_3]$–$0.85[Pb(Zr_{1/2}Ti_{1/2})O_3]$ ceramics, Ceramics International 30 (2004) 1453–1457.

[16] G. Feng, H. Rongzi, L. Jiaji, L. Zhen, T. Chang-sheng, Effects of ZnO/Li_2O codoping on microstructure and piezoelectric properties of low-temperature sintered PMN–PNN–PZT ceramics, Ceramics International 35 (2009) 1863–1869.

[17] Y. Yan, A. Kumar, M. Correa, K.H. Cho, R.S. Katiyar, S. Priya, Phase transition and temperature stability of piezoelectric properties in Mn-modified $Pb(Mg_{1/3}Nb_{2/3})O_3$–$PbZrO_3$–$PbTiO_3$ ceramics, Applied Physics Letters 100 (2012) 152902.

[18] J. Du, J. Qiu, K. Zhu, H. Ji, X. Pang, J. Luo, Effects of Fe_2O_3 doping on the microstructure and piezoelectric properties of $0.55Pb(Ni_{1/3}Nb_{2/3})O_3$–$0.45Pb(Zr_{0.3}Ti_{0.7})O_3$ ceramics, Materials Letters 66 (2012) 153–155.

[19] X. Chao, L. Yang, H. Pan, Z. Yang, Fabrication, temperature stability and characteristics of $Pb(Zr_xTi_y)O_3$–$Pb(Zn_{1/3}Nb_{2/3})O_3$–$Pb(Ni_{1/3}Nb_{2/3})O_3$ piezoelectric ceramics bimorph, Ceramics International 38 (2012) 3377–3382.

[20] Y.T. Chen, S.C. Lin, S.Y. Cheng, Temperature dependence of dielectric and piezoelectric properties of PLZT–PZN ceramic tapes, Journal of Alloys and Compounds 449 (2008) 101–104.

[21] C.C. Tsai, C.S. Hong, C.C. Shih, S.Y. Chu, Electrical properties and temperature behavior of ZnO-doped PZT–PMnN modified piezoelectric ceramics and their applications on therapeutic transducers, Journal of Alloys and Compounds 511 (2012) 54–62.

[22] C.C. Tsai, S.Y. Chu, C.S. Hong, S.F. Chen, Effects of ZnO on the dielectric, conductive and piezoelectric properties of low-temperature-sintered PMnN–PZT based hard piezoelectric ceramics, Journal of the European Ceramic Society 31 (2011) 2013–2022.

[23] C.W. Ahn, H.C. Song, S. Nahm, S. Priya, S.H. Park, K. Uchino, H.G. Lee, H.J. Lee, Effect of ZnO and CuO on the sintering temperature and piezoelectric properties of a hard piezoelectric ceramic, Journal of the American Ceramic Society 89 (2006) 921–925.

[24] M.S. Yoon, Y.M. Kim, S.Y. Kweon, T.W. Hong, Y.G. Lee, S.L. Ryu, I.H. Kim, H.J. Kim, S.C. Ur, Effects of ZnO on the piezoelectric properties of $Pb(Mn_{1/3}Sb_{2/3})O_3$–$Pb(Zr,Ti)O_3$ ceramics, Journal of Electroceramics 18 (2007) 73–75.

[25] J.Y. Ha, J.W. Choi, C.Y. Kang, D.J. Choi, H.J. Kim, S.J. Yoon, Effects of ZnO on piezoelectric properties of 0.01PMW–0.41PNN–0.35PT–0.23PZ ceramics, Materials Chemistry and Physics 90 (2005) 396–400.

[26] F. Rubio-Marcos, J.J. Romero, M.G. Navarro-Rojero, J.F. Fernandez, Effect of ZnO on the structure, microstructure and electrical properties of KNN-modified piezoceramics, Journal of the European Ceramic Society 29 (2009) 3045–3052.

[27] X. Pang, J. Qiu, K. Zhu, J. Du, Effect of ZnO on the microstructure and electrical properties of $(K_{0.5}Na_{0.5})NbO_3$ lead-free piezoelectric ceramics, Journal of Materials Science Materials in Electronics 23 (2012) 1083–1086.

[28] R. Hayati, A. Barzegar, Microstructure and electrical properties of lead free potassium sodium niobate piezoceramics with nano ZnO additive, Materials Science and Engineering B 172 (2010) 121–126.

[29] B.K. Gan, K. Yao, X. He, Complex oxide ferroelectric ceramics $Pb(Ni_{1/3}Nb_{2/3})O_3$–$Pb(Zn_{1/3}Nb_{2/3})O_3$–$Pb(Mg_{1/3}Nb_{2/3})O_3$–$PbZrO_3$–$PbTiO_3$ with a low sintering temperature, Journal of the American Ceramic Society 90 (2007) 1186–1192.

[30] J.S. Pan, X.W. Zhang, Structural phase-transition region and electrical properties of $Pb(Ni_{1/3}Nb_{2/3})O_3$–$Pb(Zn_{1/3}Nb_{2/3})O_3$–$PbTiO_3$ ceramics, Journal of Applied Physics 99 (2006) 034106.

[31] N. Luo, Q. Li, Z. Xia, Effect of $Pb(Fe_{1/2}Nb_{1/2})O_3$ modification on dielectric and piezoelectric properties of $Pb(Mg_{1/3}Nb_{2/3})O_3$–$PbZr_{0.52}Ti_{0.48}O_3$ ceramics, Materials Research Bulletin 46 (2011) 1333–1339.

[32] Q.M. Zhang, H. Wang, N. Kim, L.E. Cross, Direct evaluation of domain-wall and intrinsic contributions to the dielectric and piezoelectric response and their temperature dependence on lead zirconate–titanate ceramics, Journal of Applied Physics 75 (1994) 454–459.